Current Optics and Photonics
Vol. 4, No. 3, June 2020, pp. 193-199

ISSN: 2508-7266(Print) / ISSN: 2508-7274(Online)
DOI: https://doi.org/10.3807/COPP.2020.4.3.193

Dark Field Digital Holographic Microscopy Based on Two-lens 360-degree Oblique Illumination

Xiuying Zhang[1]*, Yingchun Zhao[2], Caojin Yuan[3], Shaotong Feng[3], and Lin Wang[4]

[1]*Institute of Advanced Materials, Nanjing Tech University, Nanjing 211816, China*
[2]*Changzhou Xingyu Automotive Lighting System Co. Ltd., Changzhou 213022, China*
[3]*Key Laboratory for Opto-Electronic Technology of Jiangsu Province, Nanjing Normal University, Nanjing 210023, China*
[4]*School of Electronic and Optical Engineering, Nanjing University of Science and Technology, Nanjing 210094, China*

(Received October 31, 2019 : revised January 4, 2020 : accepted March 15, 2020)

In this paper we propose a dark-field digital holographic microscopy system based on 360-degree oblique illumination. This setup is constructed without using a dark-field objective. The principle of 360-degree oblique illumination of vortex beam and dark-field digital holographic microscopy are introduced theoretically and experimentally. By analyzing the reconstructed image of a dark-field digital hologram of a USAF 1951 target, it is proved that the imaging resolution can be improved by this method. And also, comparison and analysis are made on the reconstructed image of a bright-dark field digital hologram of a pumpkin stem slice, the result shows that the imaging contrast is also enhanced with this method, and it is effective for dark-field digital holographic microscopy imaging of large transparent biological samples.

Keywords : 360-degree oblique illumination, Dark-field microscopy, Digital holography, Resolution enhancement
OCIS codes : (090.1995) Digital holography; (110.0180) Microscopy; (110.2945) Illumination design; (120.3620) Lens system design

I. INTRODUCTION

The microscopic imaging technology is an important technique to study life sciences, and its development has attracted much attention. The microscopes can be classified into optical microscopes and electron microscopes depending on the imaging method. For which, the optical microscopy has been widely used in medical diagnosis, biological research, education and some other fields due to its low-cost and simple operation [1, 2]. More specifically, the optical microscopes are classified into bright field microscopes, dark field microscopes, and phase contrast microscopes according to different illumination methods [3-6]. In the study of multiple phase objects such as living cells or organisms, due to their transparency, translucency and non-staining, they might not be clearly distinguished under bright-field illumination, resulting in the loss of some important details. By contrast, the dark-field microscopy can enhance the contrast of high-transparency or phase object imaging. However, the dark-field microscopic objective is relatively expensive and difficult to use in portable and low-cost experiments. We thus introduce the employing of Oblique Light (OL) in dark-field microscopy to overcome these drawbacks. The OL is one of the old-fashioned lighting techniques, which has been studied by many scientists and microscopists. The traditional oblique lighting is realized by illuminating samples with a part of the light from the condenser, also known as the off-axis illumination, which, if used properly, can improve the resolution and contrast of transparent samples [7-9].

The OL illumination technique can be classified into asymmetric oblique illumination [10] and symmetrical oblique

*Corresponding author: iamxyzhang@njtech.edu.cn, ORCID 0000-0002-7430-6008
Color versions of one or more of the figures in this paper are available online.

illumination, according to the symmetry of the illumination beam, respectively. When the object is illuminated by asymmetric oblique illumination, it will produce a pseudo-embossed effect at the edges and improve the contrast of imaging. However, in order to improve the resolution, it is necessary to design masks in specific directions. The symmetrical OL includes inverted oblique 'hollow-cone illumination' or circular oblique light (COL) [11], and due to its symmetry, it does not produce the strong pseudo-embossed effect found with OL. The oblique illumination microscopy is cheap and simple, real-time sampling can be accomplished conveniently by eyepiece or CCD cameras. Gabriel Cristbal *et al.* used special optical filters to produce oblique illumination light to evaluate the image quality of samples [12, 13]; Wataru Watanabe *et al.* exploited a LED array modulation to produce two-dimensional square oblique illumination and the output-images is similar to that of conventional dark-field microscopy. This study shows that in dark-field illumination and oblique illumination, horizontal or vertical illumination enhances the image contrast of structures along the illumination direction, whether it is oblique illumination in bright-field or in the dark-field, the contrast can be enhanced in a specific direction [14]. The oblique illumination light reported in the literature is mostly obtained by using different shapes of optical filters or modulating LED arrays [15-20], and the experiment needs to be performed by using objectives.

However, due to the fact that the illumination system usually does not match the imaging objectives, in practice some optical components (such as the size of the condenser) of the imaging objective must be changed to couple the illumination system during the experiment, which causes inconveniences to the experimental operation. In addition, the above-mentioned OL sources are mostly obtained by shaping the expanded Gaussian wave or plane wave, and only part of the total intensity can be retained, so that the illumination light intensity is weakened significantly, the illumination efficiency thus gets lower. Moreover, the beam with information is easily diffracted in the process of propagation, and the background noise is generated during imaging, which reduces the resolution of imaging.

It has been proved, based on the dark-field digital holographic microscopy illuminated by using the Laguerre-Gaussian vortex beam, the imaging resolution can be improved along with the circular symmetry direction due to the quasi-non-diffraction characteristics of Laguerre-Gaussian vortex beam and the 360-degree circular symmetry oblique 'hollow-cone illumination' provided by the convergent lens [21]. On the other hand, in order to get the complete information or a wider field of view (FOV) of the object, we need to choose a dark-field microscopic objective with small numerical aperture, because it can obtain a larger focus spot to illuminate the large transparent biological samples, and this will place restrictions on our choice of the dark-field microscopic objective.

In the view of this, exploiting the 360-degree oblique illumination characteristic of a vortex beam to produce a dark field digital holographic microscopic imaging system without a dark field microscope objective becomes especially critical. In this paper, a two-lens dark-field digital holographic microscopy based on 360-degree oblique illumination has been proposed, which takes the vortex beam as an OL, and utilizes its quasi-non-diffraction characteristics and adjustable annular size to make itself incident onto the surface of an ordinary lens. Then the annular cone after focusing by the lens is regarded as 360-degree circular symmetrical oblique illumination. Following, the dark-field digital holographic microscopic imaging of the object under circular symmetrical oblique illumination is realized, theoretical analysis and experimental research are carried out as well.

II. PRINCIPLE OF EXPERIMENT

2.1. Principle of Vortex 360-degree Oblique Illumination

The vortex beam is a kind of dark hollow annular beam with spiral phase distribution and definite angular momentum of photon orbit. Its intensity distribution is a ring structure. In this paper, the special annular light intensity is used as a 360-degree oblique illumination source, and the appropriate number of topological charges is selected according to the size of the sample and the aperture of the lens. If a plane light wave with the amplitude of 1 is irradiated on a liquid crystal Spatial Light Modulator (SLM) loaded with a spiral phase diagram, the phase of the reflected wave is modulated by the SLM. The expression of the illumination function in cylindrical coordinates is [22]

$$t(\boldsymbol{r},\theta,z=0)=E_0(\frac{r}{\sigma})^{|\ell|}\exp(-\frac{r^2}{\sigma^2})\exp(\mathrm{i}\ell\theta), \tag{1}$$

in Eq. (1), ℓ denotes the number of topological charges, σ denotes the size of the Gaussian spot, E_0 is a constant, i.e. a plane wave. $\boldsymbol{r}$ and θ is the polar coordinates of the source plane, z denotes the diffraction distance. In the plane of the emitted light, $t(\boldsymbol{r},\theta,z=0)$ is an annular light, whose energy is mainly concentrated on the main ring.

The distribution of the intensity of the vortex beams with topological charges number $\ell=5$, $\ell=20$ and $\ell=50$ were shown in Fig. 1, respectively. It can be seen that the diameter of the spot broadens with the increasing of the topological charge. Therefore, according to the size of the sample to be observed, lenses of a certain size and focal length are fixed, by changing the topological charge, the radius of the main ring of the vortex spot can be altered accordingly. If the sample is illuminated directly by the spiral annular light, there will be a large dark area in the imaging center. Therefore, we designed to use a common lens to converge the annular light and illuminate the sample, and at the plane of the convergent lens, the field of the vortex beam is

$$t(\boldsymbol{r}_{z_1},\theta,z=z_1)=-\frac{\mathrm{i}k}{2\pi z}\exp(\mathrm{i}kz)\iint t(\boldsymbol{r},\theta,z=0)\times\exp\{\frac{\mathrm{i}k}{2z}[(\boldsymbol{r}_{z_1}-\boldsymbol{r})^2]\}\mathrm{d}\boldsymbol{r}, \tag{2}$$

in which, the $\boldsymbol{r}_{z_1}$ denotes the coordinates at object plane, and z_1 is the propagation distance from the generation of vortex beam to the object. After some derivations, we finally have the field of a vortex beam with an analytical form, it reads

$$t(\boldsymbol{r}=\boldsymbol{r}_{z_1},\theta,z_1)=E_0(-\mathrm{i})^{\ell+1}(\frac{\sigma'}{\sigma})^{\ell}(\frac{r}{\sigma'})^{\ell}\exp(-\frac{r^2}{\sigma'^2})\times\exp[\mathrm{i}kz_1+\mathrm{i}\frac{2z_1}{k\sigma^2}\frac{r^2}{\sigma'^2}]\exp(\mathrm{i}\ell\theta). \tag{3}$$

In Eq. (3), the symbol of σ' can be conducted from σ, like $(\sigma')^2=\sigma^2[1+4z_1^2/(k^2\sigma^4)]$, and σ' is the size of gaussian spot in z_1 plane. In this connection, one can see that if we have a greater σ and a smaller z_1, the size of the vortex's main ring won't change too much, while the vortex beam also still keeps its annular structure. That is where the quasi-non-diffraction characteristic [23] of a vortex beam comes from.

Owing to the quasi-non-diffraction characteristic of the vortex beam, the distribution of the complex amplitude after passing through the lens and the object is set as follow:

$$I(\boldsymbol{r},\theta,z_2=0)=t(\boldsymbol{r},\theta,z_1)P(\boldsymbol{r},\theta)\exp[-\mathrm{j}k\frac{r^2}{2f}]O(\boldsymbol{r},\theta), \tag{4}$$

and with $r=f\times\tan\alpha$, transform the Eq. (4), then the following equation can be obtained

$$I(\boldsymbol{r},\theta,z_2=0)=t(\boldsymbol{r},\theta,z_1)P(\boldsymbol{r},\theta)\exp[-\mathrm{j}k\frac{r\tan\alpha}{2}]O(\boldsymbol{r},\theta). \tag{5}$$

In Eq. (5), α denotes the deflection angle of the convertgent lens to the vertical incident light, $O(\boldsymbol{r},\theta)$ denotes the transmittance of the sample, $t(\boldsymbol{r},\theta,z_1)$ denotes the complex amplitude of the incident beam propagating at a certain distance of z_1, $P(\boldsymbol{r},\theta)$ denotes the pupil function of the lens, $\exp[-\mathrm{j}k(r\tan\alpha)/2]$ denotes the function of the convergence of the lens, which is equivalent to make the

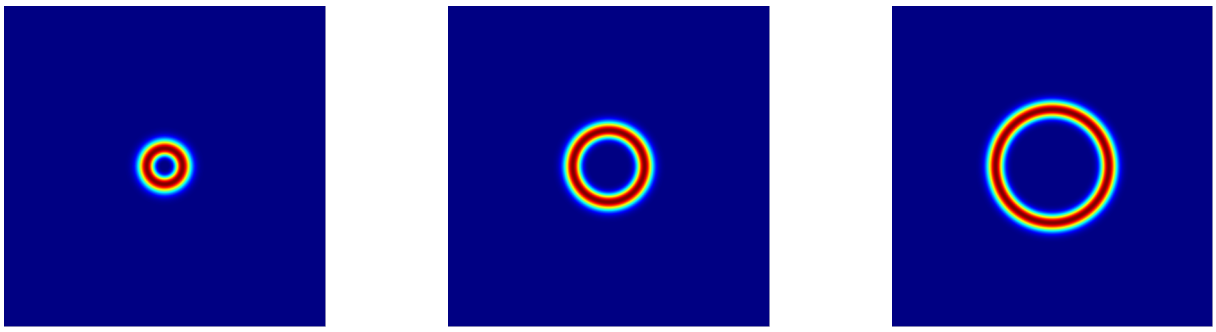

(a) (b) (c)

FIG. 1. Vortex beams with different topological charge numbers.

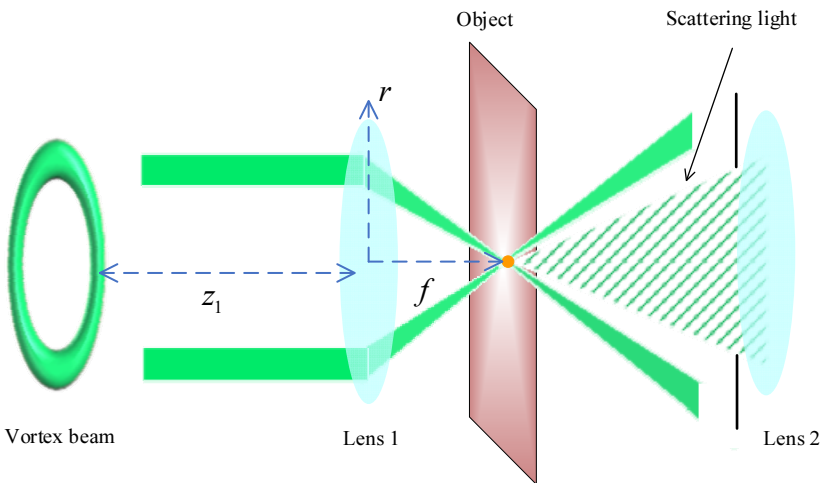

FIG. 2. Principle of 360-degree oblique illumination with vortex beam.

annular beam deflecting the angle of α, and the oblique illumination of the annular optical cone is realized, and the modulation of the Lens 1 is a z-dependent factor, while the z here equals to f, specifically, as shown in Fig. 2. In this figure, the vortex beam is focused by a lens to form an annular light cone, which can be regarded as a beam of oblique light rotating 360-degree. Therefore, when the vortex beam illuminates the object, it is equivalent to 360-degree oblique illumination.

After the object is illuminated by 360-degree oblique illumination, the beam carrying the low-frequency information of the object will be obliquely reflected in the original direction and blocked by an external aperture, not incident on the imaging lens. And the scattered light carrying the high-frequency information of the object is collected by the imaging lens along the optical axis direction, which is used to image. Thus, the dark-field microscopic imaging with 360-degree oblique illumination of the vortex beam is realized.

2.2. Principle of Dark-field Digital Holographic Microscopy

When the incident light is converged by the lens, the light becomes an annular optical cone and carries a 360-degree oblique carrier frequency, which broadens the spectral range of the recorded object to $2\alpha/\lambda$ [24]. The scattered light carrying high-frequency information of the object is imaged on the recording surface of CCD through the imaging lens and recorded as the object light. The reference light R interferes with the object light $O(\boldsymbol{r},\theta)$ on the CCD recording surface to generate a digital hologram of dark-field image plane, that is

$$H = |O(\boldsymbol{r},\theta)+R|^2 = |O(\boldsymbol{r},\theta)|^2 + |R|^2 + R^*O(\boldsymbol{r},\theta) + RO^*(\boldsymbol{r},\theta). \quad (6)$$

In Eq. (6), the superscript $(\cdot)^*$ denotes the optical conjugation. In the process of digital holographic reconstruction in dark-field, since the object light is directly imaged on the holographic recording plane, the reconstructed image does not need to calculate the spatial diffraction propagation, but is directly located on the holographic plane. However, in order to eliminate the interference of zero-order and conjugate terms, the frequency-domain filtering method is used to extract the positive (or negative) first-order spectrum in the frequency domain, and then inverse Fourier transform is performed to obtain the complex amplitude of the object light, which is expressed as follows:

$$O_1(\boldsymbol{r},\theta) = \mathrm{F}^{-1}[\mathrm{F}_{fil}(H)], \quad (7)$$

where F is the Fourier transform and F^{-1} is the inverse Fourier transform, and the subscript "*fil*" denotes a spectrum filtering operation.

III. EXPERIMENTAL SYSTEM AND RESULT ANALYSIS

3.1. Experimental System

The experimental device shown in Fig. 3 is a Mach-Zehnder interferometric optical path. In the experiment, a beam of light emitted by the laser is split into two paths by the beam splitter BS 1, and the light reflected by the beam splitter BS 1 passes through the beam expanding

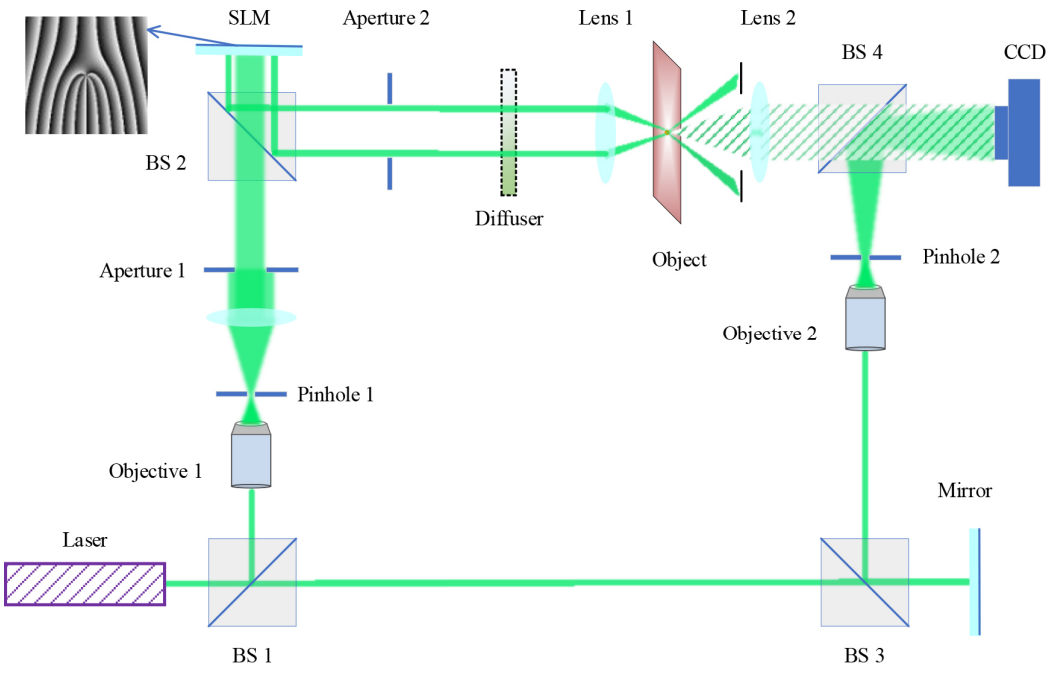

FIG. 3. Dark-field digital holographic microscopy system based on 360-degree oblique illumination.

and collimating system (Objective 1 and Pinhole 1), the Aperture 1 and the beam splitter BS 2 in turn, incident on the reflective SLM. The Aperture 1 is used to control the size of the light incident on the surface of the SLM, and the SLM is loaded with a pre-generated fork grating, and the incident light is modulated by the SLM to generate the annular vortex illumination. The Aperture 2 is used to retain the annular light and filter out the other secondary light. The retained annular vortex beam is incident to Lens 1 through a rotating scattering screen. After being focused by Lens 1, the annular cone is formed to illuminate the sample 360-degree obliquely.

Since the sample is illuminated, the scattered light is focused by Lens 2 and imaged on the surface of the CCD, that is, the object light. The reference light passes through the beam splitter BS 3 to the Mirror, and the optical path between the beam splitter BS 3 and the SLM is compensated correspondingly by adjusting the distance between the Mirror and the beam splitter BS 3, and the compensated light is transformed into a spherical wave by the beam expanding and collimating system (Objective 2 and Pinhole 2) to counteract the secondary phase factor carried by the object light in the object light path. Finally, the reference light passes through the beam splitting BS 4, interferes with object light on the surface of CCD, and the fringes were recorded as a hologram.

The laser used in the experiment is a semiconductor-pumped solid-state laser with a wave length of 532 nm and the output power is about 400 mw. The SLM is the PLUTO series of HOLOEYE, with a resolution of 1920 × 1080 pixel. The focal length of the Lens 1 is $f_1 = 2.5$ cm, the diameter of the Lens 1 is $\phi_1 = 1.27$ cm, the aperture of the Lens 1 is $d_1 = \phi_1 * 90\% = 1.143$ cm; The focal length of the Lens 2 is $f_2 = 25$ cm, the diameter of the Lens 2 is $\phi_2 = 2.54$ cm, the aperture of the Lens 2 is $d_2 = \phi_2 * 90\% = 2.286$ cm, the curvature radius of the Lens 2 is $R_2 = 25.7$ cm, and all the lenses used are uncoated. The numerical aperture of the Lens 2 can be calculated by: $NA = n * \sin\theta = n_{air} * d_2 / \sqrt{4f_2^2 + d_2^2}$, which gives us the numerical aperture of the Lens 2 being about 0.0456. The resolution limit is determined by $D = 0.82\frac{\lambda}{NA}$ [25], which is used to calculate the resolution limit of the system. So that the theoretical resolution limit of the system is 9.552 μm. One USAF 1951 target and a pumpkin stem slice are used as samples in the experiment.

3.2. Results and Analysis

Firstly, the USAF 1951 target is used as the experimental sample to obtain the reconstructed image of the dark-field hologram, as shown in Fig. 4, Fig. 4(a) is the reconstructed image of the single dark-field hologram without speckle field; Fig. 4(b) is the average value of superposition of reconstructed images of multiple holograms with speckle field. The speckle field [26-28] is formed by rotating the scattering screen (diffuser) in front of Lens 1. Multiple holograms are collected by rotating the scattering screen to multiple angles. By comparing the Figs. 4(a) and 4(b), we can see that it can effectively suppress the speckle noise caused by coherent light and improve the imaging quality. And it can be seen from the dotted line box in Fig. 4(b) that the system can distinguish the sixth group of fringes in unit 6 of the USAF 1951 target, and the corresponding resolution is 114 lp/mm, that is to say, the resolution of the system can reach 8.7 μm. This is lower than the limit resolution of bright field illumination, so this method improves the resolution of the imaging system.

Then, one pumpkin stem slice is used as experimental sample to obtain the reconstructed image of the bright and dark field hologram, as shown in Fig. 5. Figure 5(a) is the bright-field hologram of the sample without speckle field, which is obtained by replacing the annular vortex illumination with ordinary Gaussian beam illumination in Fig. 3, and Fig. 5(b) is the dark-field hologram of the sample with speckle field. Similarly, we collected multiple holograms by rotating the scattering screen (diffuser) in front of Lens 1 to multiple angles. Figure 5(c) is the

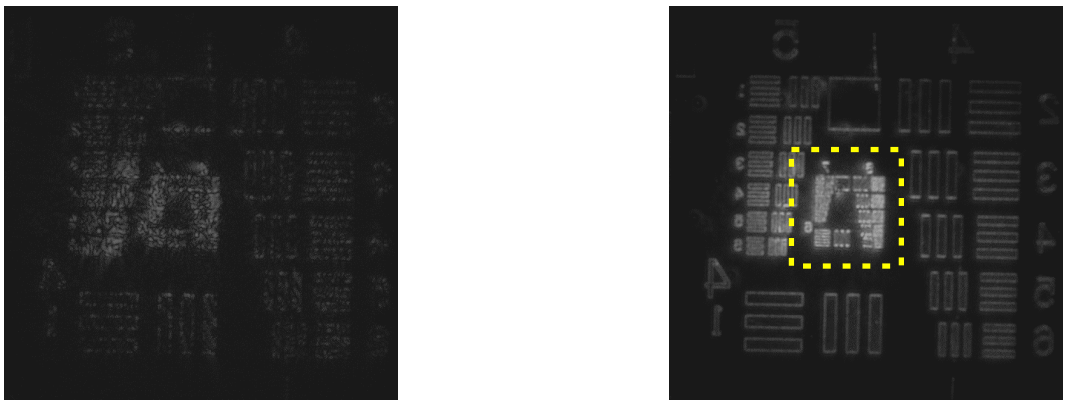

(a) (b)

FIG. 4. Reconstructed image of dark-field hologram of USAF 1951 target. (a) Reconstructed image of single hologram of USAF 1951 target without speckle field. (b) Average of reconstructed images of multiple holograms of USAF 1951 target with speckle field.

reconstructed image of a single bright-field hologram, while Fig. 5(d) is the image obtained by the average value of superposition of reconstructed images of 60 dark-field holograms. The purpose of this is to eliminate the speckle noise in the dark-field hologram. By comparing the reconstructed images in the dotted line boxes of Figs. 5(c) and 5(d), it can be seen that the background noise of the reconstructed image in bright-field is much stronger, the outline of the sample is blurred, while the background of the reconstructed image in dark-field is dark, only the sample itself is clearly visible.

With the results in Figs. 4 and 5, we firstly see a reconstruction with better contrast by our proposed system, and then a higher spatial resolution beyond the imaging system has been achieved. Specifically, the Signal to Noise Ratio (SNR) of Fig. 4(b) compared to Fig. 4(a) is increased 12.5 dB, and the SNR of Fig. 5(d) compared to Fig. 5(b), Fig. 5(c), are increased 10.7 dB and 9.36 dB, respectively. These improvements are given all thanks to the combination of the deployment of dark field illumination, the quasi-non-diffraction property of the vortex beam and the superposition of multiple holograms. All in all, compared with the conventional dark-field holography based on dark-field microscopic objective, it is proved that our method is flexible and suitable for the imaging of large-scale objects in dark-field digital holography.

IV. CONCLUSION

A two-lens dark-field digital holographic microscopy based on 360-degree oblique illumination is presented, which makes the use of the quasi-non-diffraction characteristics and the adjustability of annular intensity of a vortex beam. We propose this method which requires neither special filters, masks or LED arrays, nor needs the expensive and un-adjustable dark-field microscopic objectives. It can be accomplished by using only two ordinary lenses. What's more, unlike the previous oblique illumination and dark-field imaging, the dark-field imaging with 360-degree circular symmetrical oblique illumination is simpler and easier to operate, which reduces the experimental cost, in addition, according to the actual size of the sample, suitable lenses can be selected, and fork gratings with different topological charges can be loaded by spatial light modulator to generate different sizes of vortex rings. The study of dark-field

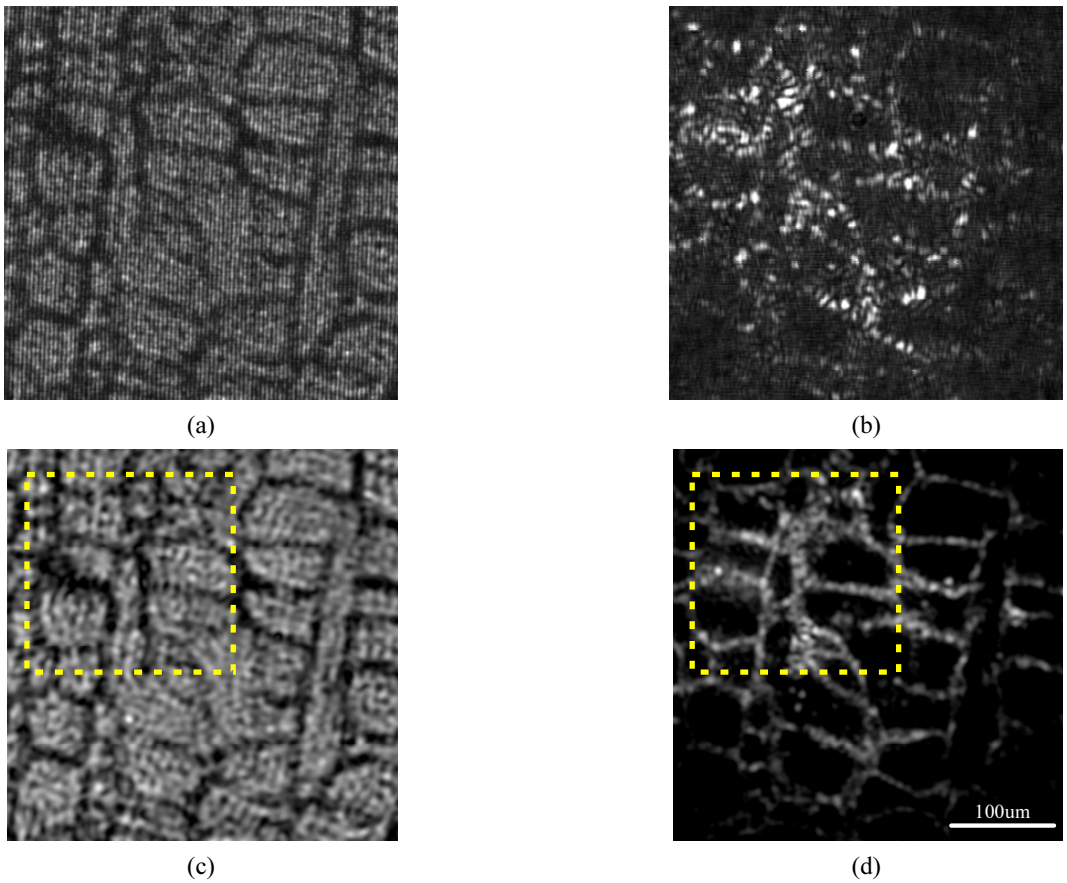

(a) (b) (c) (d)

FIG. 5. Bright-dark field hologram and reconstructed image of a pumpkin stem slice. (a) Bright-field hologram of pumpkin stem slice (b) Dark-field hologram of pumpkin stem slice (c) Reconstructed image of bright-field of pumpkin stem slice (d) Reconstructed image of dark-field hologram of pumpkin stem slice.

digital holographic microscopy with 360-degree circular symmetrical oblique illumination for large transparent biological samples is carried out by matching lenses according to vortex beams. The results show that the imaging method of two-lens dark-field digital holographic microscopy with 360-degree oblique illumination of vortex beam is better than that of an ordinary Gaussian beam's illumination in bright-field digital holographic microscopy, and both the contrast and spatial resolution of the imaging system are improved simultaneously. When compared with the conventional oblique illumination, the resolution of the assembly system in the direction of circular symmetry is improved, and the resolution is higher than 8.7 μm. Therefore, the dark-field digital holography based on two-lens 360-degree oblique illumination of a vortex beam provides a new method for dark-field digital holography, which broadens the application and research scope of dark-field digital holography, and makes it have a broader prospect in practical applications.

ACKNOWLEDGMENT

This study was supported by the National Natural Science Foundation of China (No. 61775097).

REFERENCES

1. J. Mertz, *Introduction to Optical Microscopy*, 2nd ed., (Cambridge University Press, New York, USA, 2019).
2. C. J. R. Sheppard, "Microscopy overview," in *Encyclopedia of Modern Optics*, 2nd ed., B. D. Guenther, ed. (Elsevier, Oxford, UK, 2004), Vol. 3, pp. 61-68.
3. F. Zernike, "Phase contrast, a new method for the microscopic observation of transparent objects part II," Physica **9**, 974-980 (1942).
4. C. R. Burch and J. P. P. Stock, "Phase-contrast microscopy," J. Sci. Instrum. **19**, 71 (1942).
5. G. M. Nomarski, "Differential microinterferometer with polarized waves," J. Phys. Radium **16**, 9S (1955).
6. J. Sanderson, "Contrast enhancement techniques for light microscopy," in *Cell Biology: A Laboratory Handbook*, 2nd ed., J. E. Cells, ed. (Academic Press, San Diego, USA, 1998), Vol. 3, pp. 15-33.
7. B. Kachar, "Asymmetric illumination contrast: a method of image formation for video light microscopy," Science **227**, 766-768 (1985).
8. Z. Hostounský and R. Pelc, "An efficient way of high-contrast, quasi-3D cellular imaging: Off-axis illumination," J. Biochem. Biophys. Methods **68**, 23-30 (2006).
9. T. Stephanides, *The Microscope and the Practical Principles of Observation* (Faber and Faber, London, UK, 1947).
10. C. W. Olliver, *The Intelligent Use of the Microscope*, (Chapman and Hall, London, UK, 1947).
11. W. W. Mathews, "The use of hollow-cone illumination for increasing image contrast in microscopy," Trans. Am. Microsc. Soc. **72**, 190-195 (1953).
12. J. R. Santaquiteria, J. L. E. Aranda, O. Deniz, C. Sanchez, M. B. Ramos, S. Blanco, G. Cristobal, and G. Bueno, "Low-cost oblique illumination: an image quality assessment," J. Biomed. Opt. **23**, 016001 (2018).
13. C. Sanchez, G. Cristóbal, G. Bueno, S. Blanco, M. B. Ramos, A. Olenici, A. Pedraza, and J. R. Santaquiteria, "Oblique illumination in microscopy: A quantitative evaluation," Micron **105**, 47-54 (2018).
14. R. Sugimoto, R. Maruyama, Y. Tamada, H. Arimoto, and W. Watanabe, "Contrast enhancement by oblique illumination microscopy with an LED array," Optik **183**, 92-98 (2019).
15. T. N. Ford, K. K. Chu, and J. Mertz, "Phase-gradient microscopy in thick tissue with oblique back-illumination," Nat. Methods **9**, 1195-1197 (2012).
16. T. N. Ford and J. Mertz, "Video-rate imaging of microcirculation with single-exposure oblique back-illumination microscopy," J. Biomed. Opt. **18**, 066007 (2013).
17. E. Chen and R. Wu, "Design of freeform reflector array for oblique illumination in general lighting," Opt. Eng. **54**, 065103 (2015).
18. P. Ledwig, M. Sghayyer, J. Kurtzberg, and F. E. Robles, "Dual-wavelength oblique back-illumination microscopy for the non-invasive imaging and quantification of blood in collection and storage bags," Biomed. Opt. Express **9**, 2743-2754 (2018).
19. M. Kumar and Y. Kozorovitskiy, "Tilt-invariant scanned oblique plane illumination microscopy for large-scale volumetric imaging," Opt. Lett. **44**, 1706-1709 (2019).
20. Y. Ma, S. Guo, Y. Pan, R. Fan, Z. J. Smith, S. Lane, and K. Chu, "Quantitative phase microscopy with enhanced contrast and improved resolution through Ultra-Oblique Illumination (UO-QPM)," J. Biophotonics **12**, e201900011 (2019).
21. Y. C. Zhao, X. Y. Zhang, C. J. Yuan, S. P. Nie, Z. Q. Zhu, L. Wang, Y. Li, L. P. Gong, and S. T. Feng, "Dark-field digital holographic microscopy by using vortex beam illumination," Acta Phys. Sin. **63**, 224202 (2014).
22. P. F. Ding and J. X. Pu, "Propagation of Laguerre-Gaussian vortex beam," Acta Phys. Sin. **60**, 094204 (2011).
23. G. J. Fang, S. H. Sun, and J. X. Pu, "Experimental study on fractional double-vortex beams," Acta Phys. Sin. **61**, 064210 (2012).
24. C. Yuan, G. Situ, G. Pedrini, J. Ma, and W. Osten, "Resolution improvement in digital holography by angular and polarization multiplexing," Appl. Opt. **50**, B6-B11 (2011).
25. M. Born and E. Wolf, *Principles of Optics*, 7th ed. (Cambridge University Press, Cambridge, UK, 1999).
26. Y. Park, W. Choi, Z. Yaqoob, R. Dasari, K. Badizadegan, and M. S. Feld, "Speckle-field digital holographic microscopy," Opt. Express **17**, 12285-12292 (2009).
27. B. K. Wilson and G. D. Vigil, "Automated bacterial identification by angle resolved dark-field imaging," Biomed. Opt. Express **4**, 1692-1701 (2013).
28. A. Faridian, G. Pedrini, and W. Osten, "Opposed-view dark-field digital holographic microscopy," Biomed. Opt. Express **5**, 728-736 (2014).